Research Article | Vol. 30, No. 21 / 10 Oct 2022 / Optics Express 38139
Optics EXPRESS

Eyebox uniformity optimization over the full field of view for optical waveguide displays based on linked list processing

SHUFENG YAN,[1,2,*] ENQI ZHANG,[1,2] JUNDA GUO,[1] PING JIA,[1,2] KUN YANG,[3] AND LINGSHENG KONG[1,4]

[1]Changchun Institute of Optics, Fine Mechanics and Physics, Chinese Academy of Sciences, No. 3888 Dong Nanhu Road, Changchun 130033, China
[2]University of Chinese Academy of Sciences, Beijing 100049, China
[3]Army Academy of Armored Forces, Beijing 100072, China
[4]lingshengkong@hotmail.com
[*]shufeng.yan@foxmail.com

Abstract: Eyebox uniformity is an important indicator to evaluate the performance of optical waveguide displays. However, there is currently no standard design approach that achieves ideal uniformity over the full field of view (FOV) within the eyebox. Here, a novel method for eyebox uniformity optimization based on linked list processing is proposed. The linked list processing method can fast record the light trajectory and calculate the optimal numerical diffraction efficiency distribution of the coupler. We use the linked list method for an L-shaped diffractive optical waveguide and solve the matched coupler structure by combining rigorous coupled-wave analysis (RCWA) and the simplex method. By building the model on LightTools and demonstrating the illuminance uniformity, the feasibility of the method is verified. In the FOV range of 15°× 15°, the eyebox uniformity reaches 0.9 at the central viewing angle and the overall eyebox uniformity is 0.617.

1. Introduction

Optical waveguides are currently the mainstream technical solutions for AR/MR displays [1–3], and have been used as display modules for AR helmets [4–7] and AR-HUDs [8–11]. Compared to other display technology solutions, such as freeform prisms [12–14], which have excellent performance in aberration correction but difficulty in reducing thickness, and birdbath [15], which can achieve a large field of view but its structure is unacceptable bulky, the optical waveguide is unparalleled in thinness and lightness, meanwhile, it can easily achieve a large size of eyebox through exit pupil expansion. However, with each replication of exit pupils, the beam carries part of the energy to propagate in the original direction, which causes the energy of the diffracted light to decrease. This results in poor illumination uniformity within the eyebox and low utilization efficiency of the light energy. Generally, the eyebox uniformity can be improved by redistributing the local diffraction efficiencies of the coupler, while precise regulation is not easy. One of the representative products of AR glasses, Microsoft's Hololens 2, according to the evaluation results of Karl Guttag [16], has obvious vignetting areas in the output image.

In recent years, some meaningful work has been done on the regulation of optical waveguide couplers [17–21]. The most common method is to divide the coupler into several sub-regions with equal area, and use the uniformity at the central viewing angle as the objective function to calculate the diffraction efficiency of each sub-region [19,22]. The uniformity achieved by this method improves as the number of segmented sub-regions increases. On the basis of dividing the coupler into equal parts, Liu [17] samples the full FOV, and accumulates the standard deviation of the output light intensity as the objective function to solve the diffraction efficiency distribution.

#472089 https://doi.org/10.1364/OE.472089
Journal © 2022 Received 31 Jul 2022; revised 15 Sep 2022; accepted 16 Sep 2022; published 29 Sep 2022

Optics EXPRESS

However, when the FOV range is large, this method becomes no longer effective due to the large difference in the number of exit pupils between the central and edge FOV. The essential reason is that only one diffraction efficiency is set within each sub-region, which means that the diffraction efficiency does not vary with the light propagation angle. From another perspective, eyebox uniformity optimization may be limited by the fact that existing optical software uses non-sequential ray tracing to simulate the optical waveguide. The optical waveguide is like a black box that only output field is obtained, but no information about the light field inside the optical waveguide can be extracted.

In this article, we introduce a brand new method to replace non-sequential ray tracing when optimization. According to the characteristics of the exit pupil expansion, we use linked list to record coordinates of the points where light beams contact with the coupler surface. Through numerical processing of the nodes, precise solutions of the diffraction efficiency distribution at different viewing angles are calculated, and the relationship between the diffraction efficiency and the propagation angle at each node position is obtained. We choose slanted gratings as the couplers, and optimize the specific structure of the gratings in combination with RCWA and the simplex method to satisfy the relationship. We build an L-shaped diffractive optical waveguide model on LightTools, use Rsoft to calculate the bidirectional scattering distribution function (BSDF) of the optimized slanted gratings and add it to LightTools as parameters of the coupler surface. It turns out that our method achieves relatively uniform illumination within the eyebox over the full FOV. This work provides a systematically powerful approach for the optimal design of optical waveguide couplers.

2. Linked list processing method

Light propagation trajectories inside the optical waveguide can be represented by contact points of the light beam on the surface of the waveguide. The spacing between adjacent contact points δs is determined by the thickness of the waveguide t and the direction of the wave vector. Taking the waveguide plane as the x-y plane to establish a spherical coordinate system, the spacing can be expressed as

$$\delta s = 2t \tan\theta, \tag{1}$$

where θ is the angle between the wave vector and the z-axis. If we simplify the optical waveguide structure to couplers and a glass substrate, these contact points can be classified into two cases:

Case 1. Belong to the coupler zone where the light beam interacts with the coupler. In this case the subsequent propagation direction is determined by the structure of the coupler, while the wave vector can be calculated using the grating equation,

$$k' \sin\theta' \cos\phi' = k \sin\theta \cos\phi + m_x \frac{2\pi}{d_x}, \tag{2}$$

$$k' \sin\theta' \sin\phi' = k \sin\theta \sin\phi + m_y \frac{2\pi}{d_y}. \tag{3}$$

Here m_x, m_y, d_x and d_y are the diffraction orders and periods of the coupler in the x and y directions, respectively.

Case 2. Belong to the non-coupler zone where the light beam interacts with the substrate. In this case the light beam is totally reflected without changing the subsequent propagation direction. Therefore, the wave vector should satisfy the total internal reflection condition,

$$k \sin\theta > k_0 n^{air}, \tag{4}$$

where $k_0 n^{air}$ is the wave vector in the air.

Therefore, when the incident light angle is determined, the position of all the contact points are also determined. The data structure of linked lists is quite suitable for recording contact

Optics EXPRESS

points. A linked list consists of nodes and connection between nodes. Nodes are used to record parameters including coordinates of contact points and diffraction efficiencies at that location, while the connection between nodes are used to point in the direction of the light propagation. A linked list can be a single-linked list or an adjacency linked list, depending on the number of diffraction orders used. Strictly speaking, couplers such as relief gratings or holographic gratings have high-order diffraction, but in optical waveguides they are usually optimized to concentrate their diffraction energy in two or a limited number of diffraction orders. Therefore, only main diffraction orders need to be set to the linked lists.

We apply the linked list method to Levola's classical optical waveguide layout [23] for illustration. Fig. 1(a) shows the basic structure of the layout, including an input coupler, a fold coupler and an output coupler, which are arranged in sequence. For the fold coupler and the output coupler, their −1st order diffraction and 0th order diffraction are utilized. The optical path in Fig. 1(a) corresponds to an obliquely incident beam, and it can be seen that in each coupler region, there are limited contact points on the surface. We use an adjacency linked list to record the fold coupler, as shown in Fig. 1(b), and single-linked lists to record the output coupler, as shown in Fig. 1(c). Each node of the linked list consists of two sets of data. One is the coordinate of the contact point and the other is the −1st order diffraction efficiency $\eta_{i,j}$ at that position. Since only two diffraction orders are used, the sum of energy to be distributed to these two diffraction orders should be as high as possible. Therefore, the 0th order diffraction efficiency η_0 is set by the following condition,

$$\eta_0 + \eta_{i,j} = 1, \tag{5}$$

which also simplifies the data storage of the linked list.

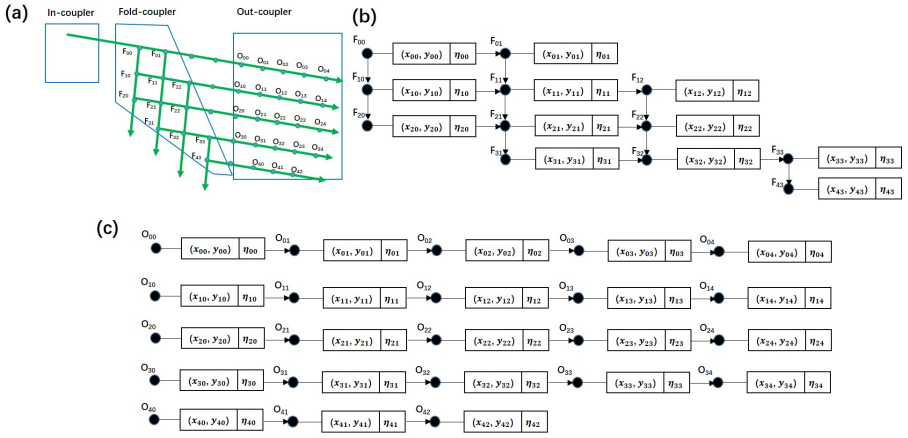

Fig. 1. Using Linked list method to record the light propagation trajectory. (a)Levola's classical optical waveguide layout. (b)An adjacency linked list for recording the fold coupler. (c)Single-linked lists for recording the output coupler.

Another feature of the linked list is that each node can be traced back. Using the linked list, all paths from the starting node to a certain node can be obtained, so the energy at the certain contact point can be calculated by superimposing energies from all the paths. We can use depth-first search (DFS) to find all paths in the adjacency linked list in Fig. 1(b). By multiplying the corresponding diffraction efficiencies of each node $F(k)$ in each path l, and summing the results of all paths, the residual energy I_f of the node $F_{i,j}$ can be calculated,

$$I_f(i,j) = \sum_{l=1}^{n_f(i,j)} \prod_{k\ in\ l} I_f(0,0)\eta_k, \tag{6}$$

Optics EXPRESS

where $n_f(i,j)$ is the number of paths from the starting node to the certain node $F_{i,j}$, and η_k is the -1st order or 0th order diffraction efficiency of the node $F(k)$, depending on whether changing the light propagation direction at that location.

In Fig. 1(c), each single-linked list represents an independent propagation path. The residual energy I_o of each node can be calculated by multiplying the 0th order diffraction efficiency of all nodes from the starting to the penultimate, and then multiplying the energy of the stating node $I_o(i,0)$,

$$I_o(i,j) = I_o(i,0)\prod_{k=0}^{j-1}(1-\eta_o(i,k)), \tag{7}$$

where $\eta_o(i,k)$ represents the -1st order diffraction efficiency at the position of the node $O_{i,k}$.

Here, the linked lists in Fig. 1(b) and Fig. 1(c) can be connected by the corner mark of the nodes, so as to construct a complete optical path inside the optical waveguide. Compared with the traditional non-sequential ray tracing, the advantage of the linked list method is that the distribution of the output light energy is a function of the diffraction efficiency of local positions. Through some processing methods this function can be analytical, so that the optimal diffraction efficiency distribution of the coupler can be solved precisely. The linked list method also has great flexibility. When multiple diffraction orders of a coupler are used, multiple propagation directions will be generated at the node positions, which can be recorded by adding multiple groups of branches to the main linked list. Therefore, it is also suitable for a two-dimensional coupler.

3. Optimization of illumination uniformity

3.1. Recursive solution of nodal diffraction efficiency

In this section we will show how to use linked list processing to precisely optimize illumination uniformity. Take the diffractive optical waveguide with L-shaped layout as an example. The light propagation trajectories are showed in Fig. 2(a).

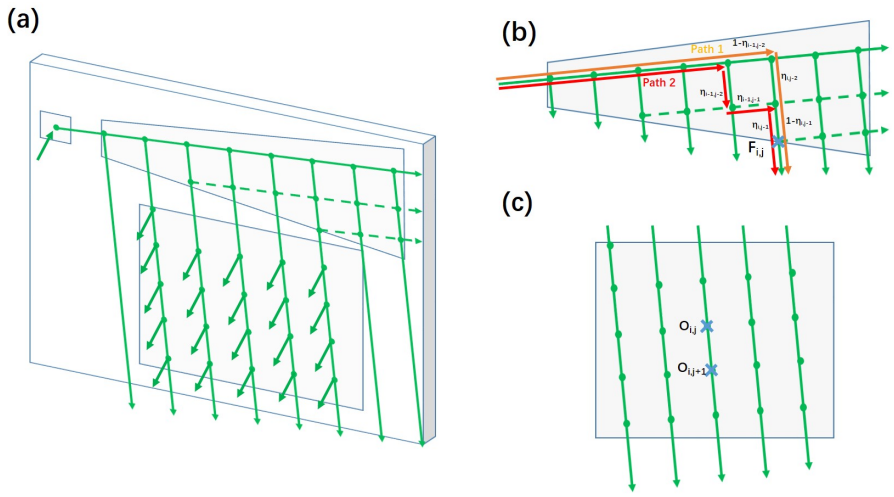

Fig. 2. Contact points on the surface of an L-shaped diffractive optical waveguide. (a)The optical path of a diffractive optical waveguide with L-shaped layout. (b)The optical path and energy distribution in the fold grating region. (c)The optical path and energy distribution in the output grating region.

Optics EXPRESS

For the linked lists of the output grating, as shown in Fig. 2(c), we take any two adjacent nodes $O_{i,j}$ and $O_{i,j+1}$. The intensity of the light coupled out from $O_{i,j}$ and $O_{i,j+1}$ should be the same. According to Eq. (7), the following relationship can be derived,

$$\eta_o(i,j) = \frac{1}{1+\frac{1}{\eta_o(i,j+1)}}. \tag{8}$$

Here, $\eta_o(i,j)$ represents the -1st order diffraction efficiency at the position of the node $O_{i,j}$.

In order to maximize the use of energy, the last node of the single-linked list requires the -1st order diffraction efficiency to be at its highest level. We can set this maximum value according to the actual grating type, so that the -1st order diffraction efficiency of the remaining nodes can be calculated by recursive Eq. (8). The above formula ensures that after pupil replication of the same column, the output light intensity is the same. Therefore, the optimization of the fold grating should be such that the total light energy transmitted to each single-linked list of the output grating is proportional to the number of nodes in the corresponding single-linked list.

For the fold grating, as shown in Fig. 2(b), we have analyzed that it is necessary to sum the light energy of all paths to obtain the residual energy of a certain node. However, when applied to the L-type optical waveguide, due to the large number of lateral pupil replication, it means that most of the energy needs to be transmitted to the subsequent nodes through the 0th order diffraction, and the -1st order diffraction efficiency is normally less than 10%. Take node $F_{i,j}$ for instance. There are two propagation paths marked in red and orange in Fig. 2(b), and the energy ratio to reach the node is

$$\frac{E_{Path2}}{E_{Path1}} = \frac{\eta_f(i-1,j-2)\eta_f(i-1,j-1)\eta_f(i,j-1)}{(1-\eta_f(i-1,j-2))\eta_f(i,j-2)(1-\eta_f(i,j-1))} < 1.23\%. \tag{9}$$

Therefore, during optimization, the energy added by the dotted propagation path in Fig. 2(a) can be ignored, thereby simplifying the calculation process of the diffraction efficiency distribution. We make the diffraction efficiency value of each column node of the adjacency list the same. According to the requirement that the light energy leaving the fold grating should be proportional to the number of nodes in the corresponding single-linked list of the output grating, we can obtain the recurrence relation of the diffraction efficiency of the adjacency list,

$$\eta_i(1-\eta_i)^{n_i-2}N_{i+1} = \eta_{i+1}(1-\eta_{i+1})^{n_{i+1}-1}N_i. \tag{10}$$

Here, n_i represents the number of nodes of the ith column of the adjacency linked list, and N_i represents the number of nodes of the ith single-linked list. Eq. (10) can be solved numerically using the least squares method. Therefore, through the linked list processing, we can obtain the distribution results of the diffraction efficiency of the fold grating and the output grating, which make the illumination absolutely uniform.

3.2. Optimization strategy over the full field of view

The illumination uniformity of the optical waveguide display is reflected in the spatial uniformity and the angular uniformity. Spatial uniformity refers to the illumination uniformity of different positions in the eyebox, while the angular uniformity refers to the illumination uniformity at different viewing angles of the same position in the eyebox. The latter can be achieved ideal uniformity by adjusting the light source, while the former can only be accomplished by optimizing the couplers. For the full FOV, the following four-step strategy is adopted to achieve spatial uniformity, which is shown in Fig. 3(a).

Step 1: Sample the incident angle of the full FOV. For incident beams with different angles, we can obtain a set of linked lists representing the light propagation trajectories inside the optical waveguide, thereby forming a three-dimensional linked list.

Optics EXPRESS

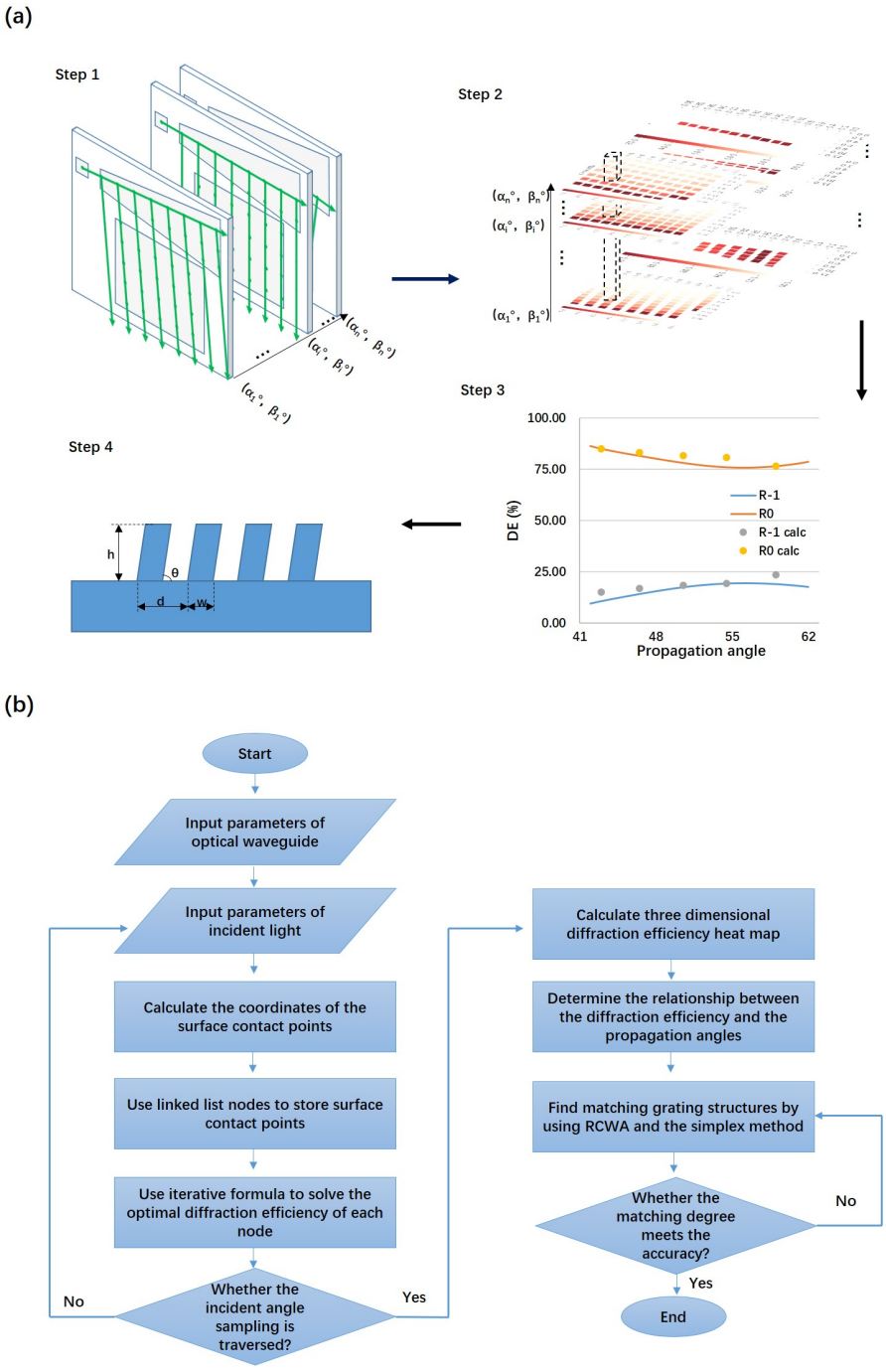

Fig. 3. Uniformity optimization method. (a)The optimization strategy to achieve spatial uniformity over the full FOV. (b)Complete flow chart for linked list processing module.

Optics EXPRESS

Step 2: Solve the three-dimensional diffraction efficiency distribution. For the three dimensional linked list in the step 1, considering that the beam has a certain diameter, we can expand the nodes into point groups. According to the algorithm in section 3.1, we can calculate the heat map of the numerical diffraction efficiency distribution corresponding to each set of linked lists, so as to obtain a three-dimensional diffraction efficiency distribution.

Step 3: Determine the relationship between the local diffraction efficiency and the propagation angle of each coupler. For every position on the coupler surface, the variation relationship between the diffraction efficiency and the incident angle can be obtained in the longitudinal axis direction. Further, the incidence angle can be converted to the propagation angle for RCWA calculation.

Step 4: Solve the specific structure of the grating according to the relationship between the diffraction efficiency and the propagation angle. Here we set the objective function as

$$F = \sum_{i=1}^{n} |Rm1_i(x_1, x_2, \ldots, x_N) - \eta_i| + |R0_i(x_1, x_2, \ldots, x_N) - 1 + \eta_i|, \tag{11}$$

where n is the number of samples of the incident angle, x_1, x_2,. . . , x_N are structure parameter variables of the grating, and η_i is the local −1st order diffraction efficiency calculated at the ith propagation angle. $Rm1_i$ and $R0_i$ represent reflective diffraction efficiencies of the −1st order and the 0th order, respectively, which can be solved by RCWA method. We use the simplex method, which can quickly solve the minimum value of the objective function in a limited parameter space, so as to obtain the corresponding grating structure parameter values.

Compared with existing methods, we chose to find the specific microstructure of the grating by matching the relationship between the diffraction efficiency and the propagation angle instead of matching average diffraction efficiency distribution over the full FOV, so that uniform illumination can be obtain at each viewing angle. This optimization strategy can theoretically achieve absolute spatial uniformity even at large FOV. But considering the optimization constraints of the actual structure of the grating, the final uniformity might drop slightly. Combined with the linked list record method, the complete flow chart is shown in Fig. 3(b). We use python to build the whole linked list processing module.

4. Simulation results and discussion

As shown in Fig. 4(a), we built a model of an L-shaped optical waveguide on LightTools. We choose the incident plane wave with wavelength of 525nm. The substrate material selected for the optical waveguide is BK7, with the refractive index of 1.52 at the wavelength of 525 nm. The thickness of the optical waveguide is 0.8 mm. Fig. 4(b) presents the analysis diagram in k domain. Due to the limitation of the refractive index of the substrate, when light propagating inside the optical waveguide, the FOV rectangle can only move within the ring with inner radium of $k_0 n^{air}$ and outer radium of $k_0 n^{ow}$. However, the distance between adjacent replicated exit pupils also needs to be considered. When the distance is too large, as the human eye moves within the eyebox, dark area may appear because light from certain viewing angles cannot enter the human eye. Therefore, we further give the bounding range of the FOV rectangle,

$$2t \tan[\arcsin \frac{k_{limit}}{k_0 n^{ow}}] - D_{beam} < D_{pupil}, \tag{12}$$

where D_{pupil} represents the diameter of the pupil of the human eye, ranging from 2 to 7 mm, and D_{beam} represents the beam diameter. When the beam diameter is 2mm, we can get $k_{limit} < 1.41 k_0$. To demonstrate the effectiveness of our proposed uniformity optimization method, we choose the largest FOV that satisfies the above constraints, which is 15°×15°. Using the grating equation, the periods of the input grating, the fold grating and the output grating can be calculated to be 448 nm, 316 nm and 448 nm, respectively.

Optics EXPRESS

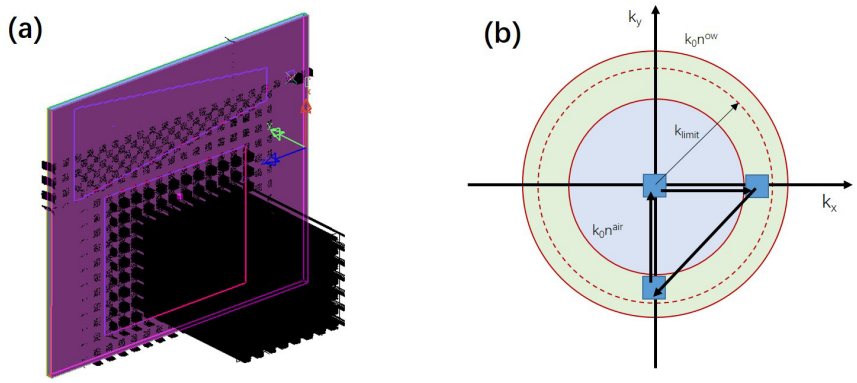

Fig. 4. The L-shaped optical waveguide. (a)Model built on LightTools. (b) K-domian analysis diagram.

We sample the full FOV by dividing the horizontal viewing angle α and vertical viewing angle β into five equal parts. For the fold grating, horizontal pupil replication determines the maximum number of pupil replication. Therefore, we divide the sub-zones of the fold grating according to the pupil replication at the edge viewing angle of $(-7.5°, 0°)$. Similarly, for the output grating, we divide the sub-zones according to the pupil replication at the edge viewing angle of $(0°, 7.5°)$. For other viewing angles, although propagation directions and pupil replication positions are different, the number of pupil replication in the grating area must be less than or equal to the number of divided sub-zones, and therefore adjacent pupil replications fall in different sub-zones. A sub-zone may be in different diffraction efficiency coverage regions, and the diffraction efficiency value of this sub-zone needs to be weighted and averaged. By using the linked list processing module, the diffraction efficiency of each sub-zone is solved. The results are shown in Fig. 5. It should be illustrated that in Fig. 5(a), the diffraction efficiency of the sub-zones 18-20 is 0 at some viewing angles. This is because the beam corresponding to the viewing angle does not enter the output grating from these sub-zones. Therefore, in these sub-zones, it is only necessary to consider the viewing angle with non-zero diffraction efficiency. From Fig. 5, we can find that for the same sub-zone, the difference in the optimal diffraction efficiency at different incident light angles increases with the increase of the angle difference. If weighted average diffraction efficiencies of all viewing angles are used to design the grating structure, it is obvious that the uniformity over the full FOV is hard to achieve, especially when the FOV range becomes larger.

We adopt the optimization strategy in section 3.2, and obtain the parameter values of slanted gratings in each sub-zone of the fold grating and the output grating, as shown in Fig. 6(a)-(c), (g)-(i), respectively. Furthermore, we calculate the diffraction efficiency curve of the slanted grating after optimization, and compare it with the optimal result in Fig. 5. The 5th, 10th, and 15th sub-zones of the fold grating (d)-(f) and the 3rd, 6th, and 9th sub-zones of the output grating (j)-(l) are selected for demonstration. It is found that in the fold grating region, the curve and scatters are well matched, and the diffraction efficiency of the slanted grating increases with the increase of the propagation angle, which is in line with our design expectations. In the output grating region, the matching degree of the curve and the scatter in the 3rd sub-zone is still high. However, in the 6th sub-zone, it can be seen that the curve does not perfectly match the scatter values. In the 9th sub-zone, the optimal diffraction efficiency corresponding to the maximum propagation angle is much higher than that corresponding to the small angle, and the diffraction efficiency of the slanted grating at the maximum propagation angle deviates significantly from the calculated results. This may be caused by the structural limitation of slanted gratings, which

Optics EXPRESS

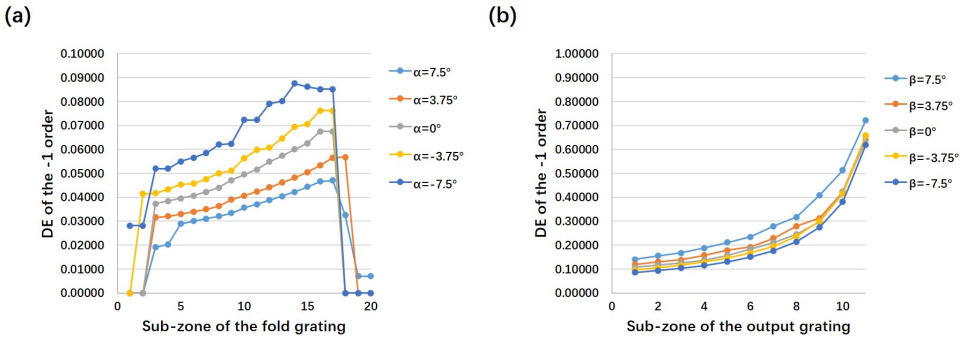

Fig. 5. Numerical solution of diffraction efficiency for each sub-zone. (a)Diffraction efficiency of each sub-zone of the fold grating with incident angles of $(7.5°, 0°)$, $(3.75°, 0°)$, $(0°, 0°)$, $(-3.75°, 0°)$ and $(-7.5°, 0°)$. (b)Diffraction efficiency of each sub-zone of the output grating with incident angles of $(0°, 7.5°)$, $(0°, 3.75°)$, $(0°, 0°)$, $(0°, -3.75°)$ and $(0°, -7.5°)$.

cannot simultaneously satisfy a large change in diffraction efficiency within a large propagation angle range.

We use Rsoft to calculate the bidirectional scattering distribution function of slanted gratings of each sub-zone and add the results as a surface parameter to the coupler region on LightTools. A surface receiver with a size of 16mm×12mm is added as an eyebox which is 20mm away from the output grating. The irradiance in the eyebox is shown in Fig. 7. It should also be noted that dividing sub-zones according to the maximum number of pupil replication is an optimization strategy that considers all viewing angles. When it comes to the manufacture, the number of sub-zones needs to be changed according to processing accuracy, time, and cost. We expect that processing capabilities will increase over time, and advanced low-cost processing technologies such as two-photon polymerization printing will be mature so that the proposed sub-zone division method can be used as an optional standard in the future.

In the simulation, in order to better demonstrate the local irradiance in the eyebox, the beam diameter is set as 1.25mm, which can avoid the overlapping of the light spots. We use a 9-point method to assess the spatial uniformity. Select 9 squares of 2mm×2mm that are evenly distributed in the eyebox and find the maximum irradiance I_i in each square as evaluation. We calculate uniformity using the following formula,

$$Uniformity = \frac{2Min(I_1, I_2, \ldots I_9)}{Max(I_1, I_2, \ldots I_9) + Min(I_1, I_2, \ldots I_9)} \tag{13}$$

The calculation result are shown in Table 1. From left to right, and from top to bottom in the eyebox, the 9 regions are numbered 1-9 in order. It is shown that the spatial uniformity at the center viewing angle is excellent (No.5), at the left edge viewing angle and upper edge viewing angle are also good (No.1, No.2 and No.4), but the spatial uniformity at other edge viewing angles are slightly worse. The right edge viewing angle and the lower edge viewing angle are corresponding to the large propagation angles in the optical waveguide. We have illustrated with Fig. 6 that at large propagation angles, the diffraction efficiency of the optimized slanted grating does not well match the calculated optimal value. If a kind of grating structure with a higher degree of freedom such as metagratings is used, we believe that a better matching degree can be achieved at large propagation angles, leading to better eyebox uniformity over a large range of FOV.

To further demonstrate overall eyebox uniformity, we replace the incident plane wave with a Lambertian surface source. The divergence half-angle of the light source is 7.5 degrees. As shown in Fig. 8, an aperture with a diameter of 4 mm and an ideal lens with a focal length of

Optics EXPRESS

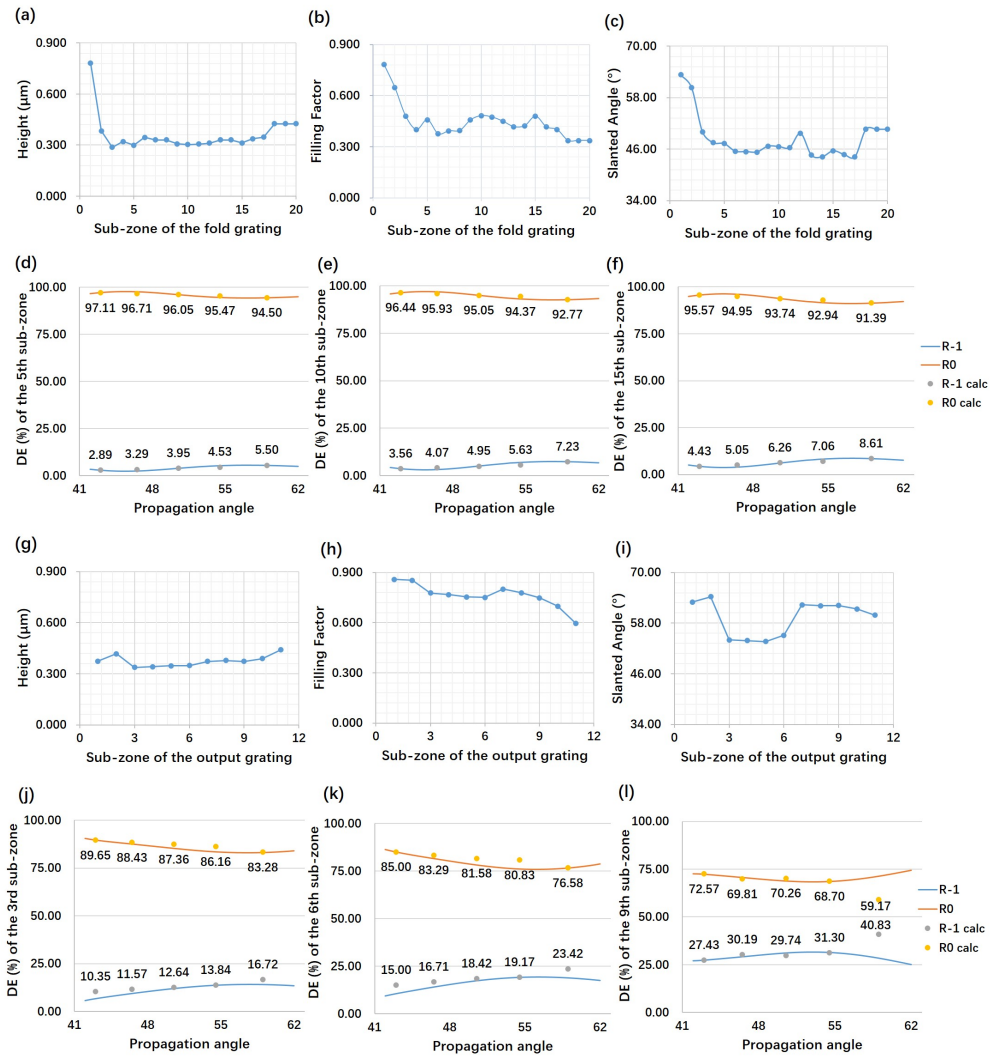

Fig. 6. Grating parameters and diffraction efficiency of each sub-zone of the fold grating and the output grating. (a)-(c),(g)-(i)Height, filling factor and slanted angle values of slanted gratings for each fold grating sub-zone and output grating sub-zone, respectively. (d)-(f),(j)-(l)The diffraction efficiency of the slanted grating of the 5th, 10th, and 15th fold grating sub-zones and the 3rd, 6th, and 9th output grating sub-zones varies with the propagation angle. Here scattered points are the optimal results calculated by the linked list processing method.

Optics EXPRESS

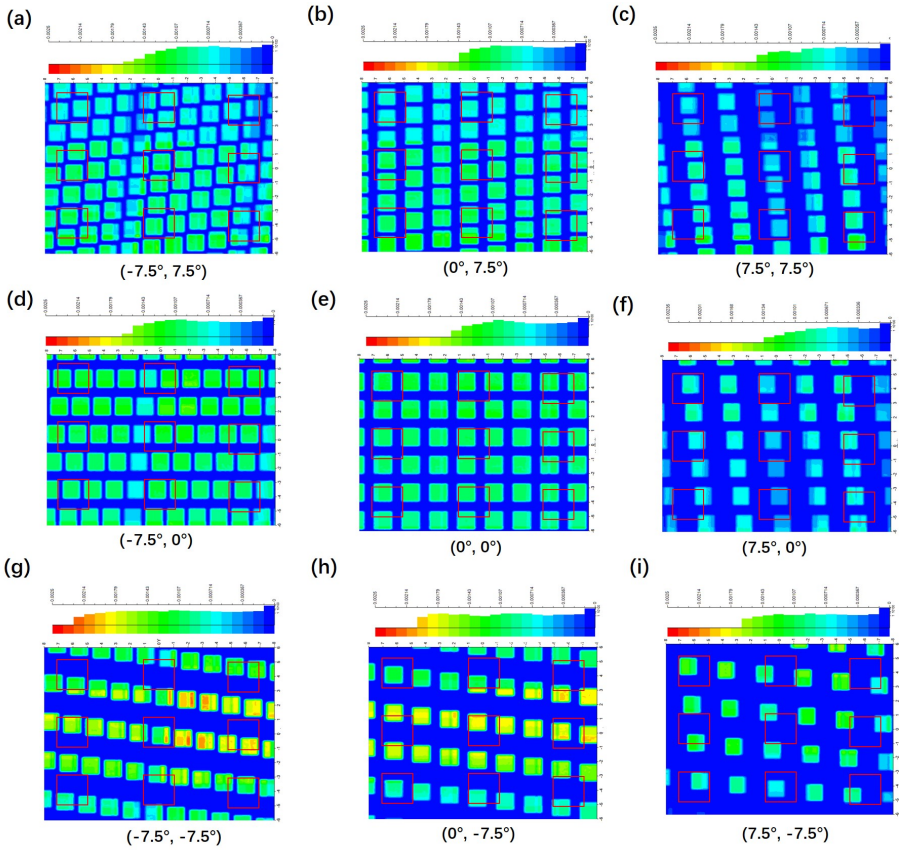

Fig. 7. The irradiance (unit:W/mm^2) in the eyebox at different viewing angles. (a)Viewing angle of $(-7.5°, 7.5°)$. (b)Viewing angle of $(0°, 7.5°)$. (c)Viewing angle of $(7.5°, 7.5°)$. (d)Viewing angle of $(-7.5°, 0°)$. (e)Viewing angle of $(0°, 0°)$. (f)Viewing angle of $(7.5°, 0°)$. (g)Viewing angle of $(-7.5°, -7.5°)$. (h)Viewing angle of $(0°, -7.5°)$. (i)Viewing angle of $(7.5°, -7.5°)$.

Table 1. The irradiance (unit:W/mm^2) and spatial uniformity at different viewing angles

No.	Viewing angle	I_1	I_2	I_3	I_4	I_5	I_6	I_7	I_8	I_9	Spatial uniformity
1	$(-7.5°, 7.5°)$	0.00080	0.00093	0.00076	0.00114	0.00133	0.00103	0.00139	0.00130	0.00121	0.70898
2	$(0°, 7.5°)$	0.00082	0.00079	0.00076	0.00117	0.00115	0.00109	0.00107	0.00143	0.00115	0.69320
3	$(7.5°, 7.5°)$	0.00062	0.00045	0.00055	0.00091	0.00066	0.00089	0.00133	0.00066	0.00130	0.50538
4	$(-7.5°, 0°)$	0.00129	0.00143	0.00128	0.00113	0.00124	0.00110	0.00102	0.00117	0.00103	0.83434
5	$(0°, 0°)$	0.00120	0.00127	0.00121	0.00106	0.00108	0.00107	0.00103	0.00106	0.00104	0.89713
6	$(7.5°, 0°)$	0.00087	0.00061	0.00096	0.00080	0.00058	0.00083	0.00067	0.00048	0.00075	0.66389
7	$(-7.5°, -7.5°)$	0.00135	0.00147	0.00144	0.00171	0.00211	0.00198	0.00099	0.00168	0.00157	0.63687
8	$(0°, -7.5°)$	0.00116	0.00152	0.00158	0.00179	0.00186	0.00198	0.00123	0.00090	0.00147	0.62667
9	$(7.5°, -7.5°)$	0.00144	0.00101	0.00071	0.00124	0.00083	0.00130	0.00090	0.00063	0.00100	0.61311

17 mm are added at a distance of 20 mm from the output grating, and the receiver is placed on the focal plane. The 9-point method is also used to detect the total power of each region in the eyebox. From left to right, and from top to bottom in the eyebox, the 9 regions are numbered 1-9

Optics EXPRESS

in order. The measured total power of each region and calculated overall eyebox uniformity are shown in the Table 2.

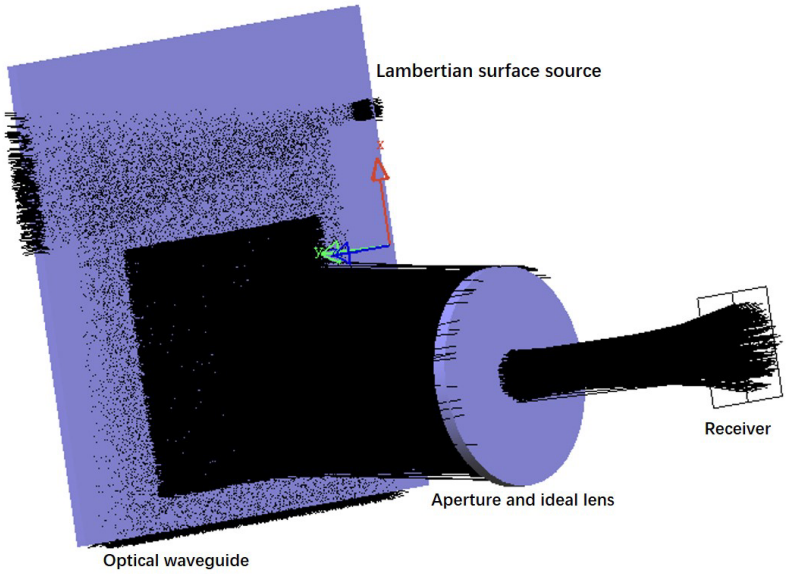

Fig. 8. Light path for overall eyebox uniformity test using a Lambertian surface source.

Table 2. The total power (unit: *W*) received at different locations and overall eyebox uniformity

I_1	I_2	I_3	I_4	I_5	I_6	I_7	I_8	I_9	Eyebox uniformity
0.00725	0.00536	0.00376	0.00737	0.00537	0.00376	0.00635	0.00456	0.00329	0.61676

5. Conclusion

In this work, a method for optimizing the eyebox uniformity of diffractive optical waveguide displays based on linked list processing is realized. According to the characteristic that light has fixed contact points on the surface of the optical waveguide, it is proposed that linked lists can be used to record the light propagation trajectory. We derive the diffraction efficiency iterative formulas, which can quickly calculate the optimal diffraction efficiency distribution of each sub-zone of the coupler. On this basis, we propose a uniformity optimization strategy for the full field of view and a design method for finding the matching grating parameters. We verified the feasibility by building an L-shaped optical waveguide on LightTools. The results show that in the FOV range of $15° \times 15°$, the eyebox uniformity reaches 0.9 at the central viewing angle, above 0.5 at the edge viewing angle. The overall eyebox uniformity is 0.617. Future work will demonstrate the application of the linked-list method to optimize eyebox uniformity in diffractive optical waveguides with more complex layouts and larger FOV. Combining with the application of metagratings, we believe that this method has the potential to achieve monolayer uniform color imaging with a large field of view.

Funding. International Cooperation Fund Project of Changchun Institute of Optics, Fine Mechanics and Physics (E20064YBQ0).

Disclosures. The authors declare no conflicts of interest.

Optics EXPRESS

Data availability. Data underlying the results presented in this paper are not publicly available at this time but may be obtained from the authors upon reasonable request.

References

1. J. Xiong, E.-L. Hsiang, Z. He, T. Zhan, and S.-T. Wu, "Augmented reality and virtual reality displays: emerging technologies and future perspectives," Light: Sci. Appl. **10**(1), 216 (2021).
2. D. Cheng, Q. Wang, Y. Liu, H. Chen, D. Ni, X. Wang, C. Yao, Q. Hou, W. Hou, G. Luo, and Y. Wang, "Design and manufacture ar head-mounted displays: A review and outlook," Light: Adv. Manuf. **2**(3), 350–369 (2021).
3. K. Yin, E.-L. Hsiang, J. Zou, Y. Li, Z. Yang, Q. Yang, P.-C. Lai, C.-L. Lin, and S.-T. Wu, "Advanced liquid crystal devices for augmented reality and virtual reality displays: principles and applications," Light: Sci. Appl. **11**(1), 161 (2022).
4. M.-U. Erdenebat, Y.-T. Lim, K.-C. Kwon, N. Darkhanbaatar, and N. Kim, *State of the art virtual reality and augmented reality knowhow* (Intechopen, 2018).
5. C. Hellmann, S. Steiner, R. Knoth, S. Zhang, and F. Wyrowski, "Physical-optics analysis of lightguides for augmented and mixed reality glasses (conference presentation)," in *Digital Optical Technologies 2019*, vol. 11062 (SPIE, 2019), p. 110620I.
6. B. C. Kress, "Optical waveguide combiners for ar headsets: features and limitations," in *Digital Optical Technologies 2019*, vol. 11062 (SPIE, 2019), p. 110620J.
7. W. Han, J.-M. Jeon, M.-H. Choi, and J.-H. Park, "Lightguide type maxwellian near-eye display with enlarged horizontal field of view by optical reconfiguration of input image," J. Inf. Disp. **23**(3), 201–211 (2022).
8. J. D. Waldern, A. J. Grant, and M. M. Popovich, "Digilens switchable bragg grating waveguide optics for augmented reality applications," in *Digital Optics for Immersive Displays*, vol. 10676 (International Society for Optics and Photonics, 2018), p. 106760G.
9. C. M. Bigler, M. S. Mann, and P.-A. Blanche, "Holographic waveguide hud with in-line pupil expansion and 2d fov expansion," Appl. Opt. **58**(34), G326–G331 (2019).
10. A. Kalinina, I. Yanusik, G. Dubinin, A. Morozov, and J.-H. Lee, "Full-color AR 3D head-up display with extended field of view based on a waveguide with pupil replication," in *Advances in Display Technologies XII*, vol. 12024 International Society for Optics and Photonics (SPIE, 2022), p. 120240D.
11. C. T. Draper and P.-A. Blanche, "Holographic curved waveguide combiner for hud/ar with 1-d pupil expansion," Opt. Express **30**(2), 2503–2516 (2022).
12. K. Pulli, "11-2: Invited paper: Meta 2: Immersive optical-see-through augmented reality," in *SID Symposium Digest of Technical Papers*, vol. 48 (Wiley Online Library, 2017), pp. 132–133.
13. F. Duerr and H. Thienpont, "Freeform imaging systems: Fermat's principle unlocks "first time right" design," Light: Sci. Appl. **10**(1), 1–12 (2021).
14. D. Cheng, J. Duan, H. Chen, H. Wang, D. Li, Q. Wang, Q. Hou, T. Yang, W. Hou, D. Wang, X. Chi, B. Jiang, and Y. Wang, "Freeform ost-hmd system with large exit pupil diameter and vision correction capability," Photonics Res. **10**(1), 21–32 (2022).
15. K. Akşit, P. Chakravarthula, K. Rathinavel, Y. Jeong, R. Albert, H. Fuchs, and D. Luebke, "Manufacturing application-driven foveated near-eye displays," IEEE Trans. Visual. Comput. Graphics **25**(5), 1928–1939 (2019).
16. K. Guttag, "Hololens 2 display evaluation part 3: Color uniformity," https://kguttag.com/2020/07/10/hololens-display-evaluation-part-3-color-uniformity/.
17. A. Liu, Y. Zhang, Y. Weng, Z. Shen, and B. Wang, "Diffraction efficiency distribution of output grating in holographic waveguide display system," IEEE Photonics J. **10**(4), 1–8 (2018).
18. D. Gu, C. Liang, L. Sun, H. Chen, Y. Chen, and L. Yang, "Optical metasurfaces for waveguide couplers with uniform efficiencies at rgb wavelengths," Opt. Express **29**(18), 29149–29164 (2021).
19. C. P. Chen, Y. Cui, Y. Chen, S. Meng, Y. Sun, C. Mao, and Q. Chu, "Near-eye display with a triple-channel waveguide for metaverse," Opt. Express **30**(17), 31256–31266 (2022).
20. S. Long, N. Li, Z. Liu, W. Chen, D. Zhang, and J. Xiao, "Color near-eye display with high exit-pupil uniformity based on optimized meta-grating," Opt. Eng. **61**(06), 065101 (2022).
21. D. Ni, D. Cheng, Y. Liu, X. Wang, C. Yao, T. Yang, C. Chi, and Y. Wang, "Uniformity improvement of two-dimensional surface relief grating waveguide display using particle swarm optimization," Opt. Express **30**(14), 24523–24543 (2022).
22. Q. Wang, Y. Zhao, and L. Zeng, "A variable profile depth crossed-grating-based exit pupil expander with improved imaging brightness uniformity," in *Holography, Diffractive Optics, and Applications XI*, vol. 11898 (SPIE, 2021), pp. 147–154.
23. T. Levola, "Diffractive optics for virtual reality displays," J. Soc. Inf. Disp. **14**(5), 467–475 (2006).